

# Comparison of Statistical and Blocky Copolymers of Ethylene Terephthalate and Ethylene 4,4'-Bibenzoate Based on Thermal Behavior and Oxygen Transport Properties

R. Y. F. LIU,<sup>1</sup> Y. S. HU,<sup>1</sup> M. R. HIBBS,<sup>2</sup> D. M. COLLARD,<sup>2</sup> D. A. SCHIRALDI,<sup>3\*</sup> A. HILTNER,<sup>1</sup> E. BAER<sup>1</sup>

<sup>1</sup> Department of Macromolecular Science and Center for Applied Polymer Research, Case Western Reserve University, 10900 Euclid Avenue, Cleveland, Ohio 44106-7202

<sup>2</sup> School of Chemistry and Biochemistry, Georgia Institute of Technology, Atlanta, Georgia 30332

<sup>3</sup> KoSa, 1551 Sha Lane, Spartanburg, South Carolina 29304

Received 22 August 2002; revised 6 November 2002; accepted 11 November 2002

**ABSTRACT:** Poly(ethylene terephthalate) (PET) was blended with a frustrated liquid-crystalline polymer, poly(ethylene terephthalate-co-4,4'-bibenzoate) (PETBB55), in the weight ratio 70:30. Under the melt conditions used for blending, NMR analysis showed that some transesterification had occurred. Accordingly, the blended product resembled a blocky copolymer more closely than it did a physical blend. A random copolymer with the same composition was synthesized for comparison. The study examined the effect of the comonomer distribution (blocky vs random) on the thermal behavior and oxygen transport properties of the glassy and cold-drawn polymers. The glass-transition temperatures and the crystallization behavior suggested that the PETBB55 blocks phase-separated as very small domains. Higher levels of orientation, as indicated by higher densities and higher trans glycol fractions, were achieved by the cold drawing of the blocky copolymer. It was speculated that the cold drawing of the blocky copolymer at temperatures up to the glass-transition temperature of the PETBB55 blocks produced highly oriented PETBB55 domains. Constraints imposed by connections between PET and the PETBB55 blocks prevented the relaxation of the continuous PET phase, even at temperatures well above the glass-transition temperature of the PET blocks. In this sense, the blocky copolymer embodied the concept of a self-reinforcing polymer. As a result, an improved oxygen barrier was obtained over a wider range of cold-draw temperatures with the blocky copolymer. © 2002 Wiley Periodicals, Inc. *J Polym Sci Part B: Polym Phys* 41: 289–307, 2003

**Keywords:** poly(ethylene terephthalate); 4,4'-bibenzoate; orientation; oxygen transport; gas permeation; polyesters; block copolymers

## INTRODUCTION

Poly(ethylene terephthalate) (PET) is widely used in a range of high barrier applications

because of its low cost and good mechanical properties. However, there is a continuing practical need to improve the barrier properties of PET. The replacement of terephthalate units by copolymerization with isophthalate, phthalate, or naphthalate reduces the gas permeability of PET.<sup>1</sup> However, the logarithmic dependence of permeability on comonomer content limits the improvement that can be expected with a small amount of comonomer.

*Present address:* \*Department of Macromolecular Science, Case Western Reserve University, Cleveland, Ohio 44106-7202

*Correspondence to:* A. Hiltner (E-mail: pah6@po.cwru.edu)

*Journal of Polymer Science: Part B: Polymer Physics*, Vol. 41, 289–307 (2003)  
© 2002 Wiley Periodicals, Inc.

Blending with a higher barrier polymer is an alternative approach. At least one example shows that blending is more effective than copolymerization in reducing the gas permeability of glassy polymers. Although copolymers of 1-trimethylsilyl-1-propyne and 1-phenyl-1-propyne exhibit the usual logarithmic dependence of gas permeability on composition,<sup>2</sup> blending poly(1-trimethylsilyl-1-propyne) with the higher barrier poly(1-phenyl-1-propyne) reduces permeability more than predicted by the logarithmic relationship.<sup>3</sup>

Very sizeable improvements in the gas barrier properties are achieved by the manipulation of the phase morphology of immiscible blends. Specialized melt processes create lamellar polyamide-6,6 domains of high aspect ratios that dramatically improve the barrier of polypropylene blends. Because of the increased tortuosity of the diffusion pathway, the lamellar morphology reduces oxygen and carbon dioxide permeability 4–5 times over that of the conventional melt blend.<sup>4</sup>

Candidate high barrier polymers for blending with PET include liquid-crystalline polymers (LCPs). Blending LCPs with PET and other thermoplastics is used to obtain advanced materials with the advantages of lower costs and the direct use of conventional melt processing equipment.<sup>5,6</sup> The intrinsically low melt viscosity and ease of orientation of LCPs often result in fibrous LCP morphologies that inspire the description of these blends as self-reinforced composites. LCPs are known to have excellent barrier properties because of their exceptionally low gas solubility.<sup>7–10</sup> However, poor processability and high cost have in general limited their applications as barrier materials. The few studies of gas transport properties in blends of a thermoplastic with an LCP indicate that the LCP phase can be considered almost impermeable in comparison with the matrix. Apparently, no attempt has been made to optimize blend morphology for barrier enhancement.

The replacement of terephthalate units with 4,4'-bibenzoate, a monomer that forms a liquid-crystalline polyester,<sup>11</sup> produces PET-based copolymers with higher glass-transition-temperature ( $T_g$ ), strength, modulus, and barrier properties.<sup>12</sup> The modulus of fibers spun from copolymers with 45–65 mol % 4,4'-bibenzoate approaches that of LCPs, and this is ascribed to the development of a frustrated liquid-crystalline structure during the spinning process.<sup>13</sup> As a quenched glass, a copolymer with 55 mol % 4,4'-bibenzoate [poly(ethylene terephthalate-

co-4,4'-bibenzoate) (PETBB55)] has an inferior gas barrier in comparison with amorphous PET.<sup>1</sup> However, the quenched glass cold-draws easily to a highly oriented film with an oxygen permeability less than one-third that of cold-drawn PET.<sup>14</sup> The decrease in permeability is due primarily to a decrease in gas solubility. The exceptional improvement in the barrier agrees with a strain-induced frustrated liquid-crystalline structure.

It is possible that blending PET with a 4,4'-bibenzoate copolymer would be more effective than copolymerization. For this purpose, PET was blended with PETBB55 in the ratio of 70:30 (w/w). Under the melt conditions used for blending, it was anticipated that some amount of transesterification would occur. Accordingly, the blended product would resemble a block copolymer more closely than it would a physical blend. The same overall 4,4'-bibenzoate concentration was also added as a monomer in the polymerization of PET to obtain the statistical copolymer. This study examined the effect of the comonomer distribution (blocky vs random) on the thermal properties and oxygen transport of the quenched and cold-drawn polymers. Correlations were sought with the conformation of the ethylene linkage, as determined by infrared spectroscopy. The solubility was analyzed with free-volume concepts developed previously.<sup>1,14</sup>

## EXPERIMENTAL

### Materials

Pellets of poly(ethylene terephthalate (PET) and statistical copolymers with 14.3 and 55 mol % terephthalate replaced with 4,4'-bibenzoate (rPETBB14.3 and PETBB55, respectively) were supplied by KoSa (Spartanburg, SC). The copolymers rPETBB14.3 and PETBB55 were polymerized from dimethyl terephthalate, dimethyl 4,4'-bibenzoate, and ethylene glycol according to the literature.<sup>15</sup> A 70:30 (w/w) blend of PET and PETBB55 (bPETBB14.3) was prepared by coextrusion in a Rheocord 90 twin-screw extruder at 285 °C.

Pellets were dried *in vacuo* at 80 °C for 24 h before molding. The dry pellets were compression-molded and quenched into amorphous films, as described previously.<sup>16,17</sup> The temperature of the press was 265 °C for PET, rPETBB14.3, and bPETBB14.3 and 290 °C for PETBB55. Films 180 and 600  $\mu\text{m}$  in thickness were prepared.

The 600- $\mu\text{m}$ -thick amorphous films were stretched under constrained uniaxial conditions, as described previously.<sup>14</sup> The specimen width before stretching was 130 mm, and the gauge length was 32 mm. Grids were marked on the specimen for measuring the draw ratio, and the specimen was clamped between wide grips and mounted in the environmental chamber of an Instron machine. Specimens were drawn at various temperatures from approximately 20 °C below the glass transition to approximately 40 °C above the glass transition. The draw rate was 5 mm min<sup>-1</sup> for PET and 2–100 mm min<sup>-1</sup> for the copolymers, depending on their response to stretching (e.g., rPETBB14.3 fractured when stretched at 85 °C if the draw rate was higher than 2 mm min<sup>-1</sup>). All the specimens were stretched to 300% to achieve a target draw ratio of 4. The actual draw ratio was determined from ink marks on the specimen. The final thickness was 100–200  $\mu\text{m}$ .

### Characterization

The coextruded blend bPETBB14.3 and the copolymer rPETBB14.3 were characterized by <sup>1</sup>H NMR spectroscopy to determine the compositions and by <sup>13</sup>C NMR spectroscopy to determine the randomness of the sequencing of the terephthalate and 4,4'-biphenylene structural units. Samples were dissolved in mixtures of deuterated trifluoroacetic acid and CDCl<sub>3</sub> (ca. 5:95 v/v), and chemical shifts were measured with respect to internal tetramethylsilane. The <sup>1</sup>H and <sup>13</sup>C spectra were acquired on a Bruker DMX 500 MHz instrument operating at 500.1 and 125.8 MHz, respectively. The spectral width was 31 kHz, the relaxation delay was 2 s, and inverse gated decoupling was used to eliminate the nuclear Overhauser effect. 4000–16,000 scans were acquired. A deconvolution program in the NMR software was used to integrate the <sup>13</sup>C spectra.

Dynamic mechanical measurements on quenched 180- $\mu\text{m}$ -thick films were carried out in a DMTA Mk II unit from Polymer Laboratories (Amherst, MA) operating in the tensile mode. The storage modulus,  $E'$ , and  $\tan \delta$  were measured at a frequency of 0.1 Hz and at a heating rate of 1 °C min<sup>-1</sup>.

Heating and cooling thermograms were obtained on 180- $\mu\text{m}$ -thick films with a PerkinElmer DSC-7 calibrated with indium and tin standards. All tests were performed in a nitrogen atmo-

sphere with heating and cooling rates of 10 °C min<sup>-1</sup>. After heating, the specimen was held at 290 °C for 3 min before the cooling scan was collected.

Wide-angle X-ray diffraction (WAXD) patterns were obtained on quenched films that were isothermally cold-crystallized at 155 °C for 4 h. Experiments were performed at ambient temperature with a Philips diffractometer in the transmission mode with Cu K $\alpha_1$  radiation and with a slit angle of 1/12°.

A density gradient column was constructed from a solution of calcium nitrate and water in agreement with ASTM D Standard 1505 Method B. The column was calibrated with glass floats of known density. Small pieces of quenched and oriented films (ca. 25 mm<sup>2</sup>) were placed in the column and allowed to equilibrate for 30 min before measurements were taken. Averages of four measurements are reported. The accuracy was  $\pm 0.0009$  g cm<sup>-3</sup>.

The conformational composition was determined with photoacoustic Fourier transform infrared spectroscopy, as described previously.<sup>14</sup> Spectra were collected at ambient temperature with a Nicolet 870 Fourier transform infrared spectrometer with an MTEC model 200 photoacoustic cell. Specimens 10 mm in diameter were cut from the film after barrier measurements. All infrared specimens were dried *in vacuo* at ambient temperature for the removal of moisture. For each specimen, 256 scans were collected at a resolution of 4 cm<sup>-1</sup> and at a mirror velocity of 0.158 cm s<sup>-1</sup>. The 1500–1400-cm<sup>-1</sup> region of the spectrum was deconvoluted into three Gaussian peaks with Origin 4.1 software. The fractions of gauche and trans glycol conformers were obtained from the appropriate peak heights.

The oxygen flux,  $J(t)$ , at 0% relative humidity, 1 atm of pressure, and 25 °C was measured with a Mocon Ox-Tran 2/20. Specimens were carefully conditioned as described previously.<sup>16</sup> Diffusivity  $D$  and permeability  $P$  were obtained by the fitting of the non-steady-state flux–time curve to the solution to Fick's second law. The thickness  $l$  of each specimen was determined from the measured density after the barrier measurement was completed. Most of the specimens were tested within 1–3 days after orientation. However, testing after 30 days produced the same flux, suggesting that the specimens were fully relaxed soon after orientation.<sup>14</sup>

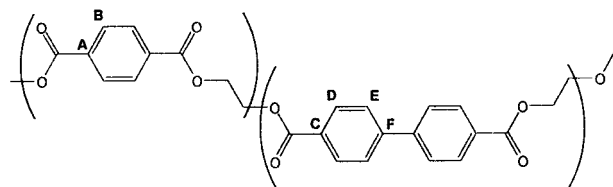
**Table 1.** Experimental and Theoretical Sequence Distribution

Material	Normalized Peak Area		<i>R</i>
	BB-BB ( $\delta = 128.77$ )	BB-T ( $\delta = 128.70$ )	
1 No transesterification <sup>a</sup>	(0.55)	(0.45)	(0.53)
bPETBB14.3			
2 As extruded #1	0.51	0.49	0.57
3 As extruded #2	0.47	0.53	0.62
4 Quenched	0.48	0.52	0.61
5 Oriented	0.49	0.51	0.60
6 At 155 °C for 4 h	0.54	0.46	0.54
rPETBB14.3			
7 Quenched	0.26	0.74	0.86
8 Oriented	0.19	0.81	0.95
9 Complete randomization <sup>a</sup>	(0.143)	(0.857)	(1.00)

<sup>a</sup> Calculated.

## RESULTS AND DISCUSSION

### Copolymer Composition and Sequence Distribution



The aromatic region of the  $^1\text{H}$  spectrum of the polymer blend has a multiplet at 8.14 ppm due to the bibenzoate protons ortho to the ester groups (D). That peak is coincident with a singlet for the terephthalate protons (B). There is another multiplet at 7.72 ppm due to the bibenzoate protons meta to the ester groups (E). By a comparison of the integrals of these three peaks, the molar ratio of terephthalate (T) to bibenzoate (BB) units for the sample prepared as a 70:30 (w/w) blend of PET and PETBB55 was found to be 85.5:14.5. The theoretical T:BB value for such a blend is 85.7:14.3, so the experimentally determined ratio is in close agreement with the expected value.

A previous study of poly(ethylene terephthalate-*co*-isophthalate) showed that the quaternary carbons of the diacid units were sensitive to sequencing and could, therefore, be used to measure the relative amounts of dyad and triad sequences.<sup>18</sup> In the  $^{13}\text{C}$  NMR spectra of bPETBB14.3 and

rPETBB14.3, there are two well-resolved peaks at 128.77 and 128.70 ppm corresponding to the ipso carbons of the bibenzoate units (C) in BB-BB and BB-T dyad sequences, respectively. The integrations of these two peaks can be used to determine the amount of transesterification that occurs during extrusion. If the two polymers did not react at all, these peaks would have an integral ratio of 55:45 for the BB-BB and BB-T dyads. If the two polymers completely randomized during extrusion, these peaks would have an integral ratio of 14.3:85.7. The ipso carbons of the terephthalate units (A) are also sensitive to the identities of neighboring diacid units, but the resulting peaks are poorly resolved and cannot be integrated quantitatively.

Table 1 shows the relative integrations of the signals for the BB-BB and BB-T dyads. Entries 1 and 9 in Table 1 show the extremes expected for unreacted and completely transesterified blends. Entries 7 and 8 confirm the statistical distribution of bibenzoate in rPETBB14.3. Entries 2 and 3 contain duplicate results for the as-extruded polymer blend. It is clear from the variation of these results that the normalized peak areas have an error of at least  $\Gamma^2$ .

If  $P_{\text{BB-T}}$  is the probability of finding a T unit next to a BB unit and  $P_{\text{T-BB}}$  is the probability of finding a BB unit next to a T unit, the degree of randomness  $R$  is defined as follows for the transesterification:<sup>19</sup>

$$R = P_{\text{BB-T}} + P_{\text{T-BB}} \quad (1)$$

Here,  $P_{\text{BB-T}}$  is the fraction of the normalized area in Table 1 for the peak at 128.70 ppm.  $P_{\text{T-BB}}$  is calculated from  $P_{\text{BB-T}}$ , and the stoichiometry of the blend is calculated as follows:

$$P_{\text{T-BB}} = (P_{\text{BB-T}})(14.3)/(85.7) \quad (2)$$

$R$  is used to describe the randomness of a PETBB copolymer:  $R = 1$  for a random copolymer,  $R = 2$  for an alternating copolymer, and  $R = 0$  for a physical blend without transesterification between PET and poly(ethylene bibenzoate) (PEBB). In the aforementioned case of blending PET homopolymer with PETBB55 copolymer in a weight ratio of 70:30, the initial mixture would have a value of  $R = 0.53$ .

Some transesterification occurred during extrusion, as indicated by  $R = 0.57\text{--}0.62$  (entries 2–3). Accordingly, the blended product resembled a block copolymer more closely than it did a physical blend. The processing of the blend into a film (entry 4) and the orientation of that film (entry 5) appeared to have no further effect on the sequence, nor did isothermal crystallization at 155 °C for 4 h (entry 6).

### Thermal Transitions and Crystallinity

The dynamic mechanical properties of quenched PET, rPETBB14.3, bPETBB14.3, and PETBB55 are compared in Figure 1. Each exhibited an intense relaxation peak in the  $\tan \delta$  curve accompanied by a large drop in  $\log E'$ . The corresponding  $T_g$ 's were 81, 89, and 106 °C for PET, rPETBB14.3, and PETBB55, respectively, as tabulated in Table 2. Because rPETBB14.3 and PETBB55 are random copolymers of ethylene terephthalate and ethylene bibenzoate,  $T_g$ 's should obey the standard copolymer equation:

$$T_g = T_{g1}w_1 + T_{g2}w_2 \quad (3)$$

where  $T_g$  is the copolymer glass-transition temperature;  $w_1$  and  $w_2$  are the weight fractions of ethylene terephthalate and ethylene bibenzoate, respectively; and  $T_{g1}$  and  $T_{g2}$  are the glass-transition temperatures of PET and PEBB, respectively. Equation 3 accurately describes the copolymer  $T_g$ 's, with  $T_{g2}$  of PEBB taken to be 122 °C.

Equation 3 does not describe the temperature of the large relaxation in the dynamic mechanical thermal analysis (DMTA) spectrum of bPETBB14.3. The peak temperature of 83 °C

was closer to the glass transition of PET than to the glass transition of rPETBB14.3. It is characteristic of blocky copolymers that they exhibit two  $T_g$ 's, which are close to the transition temperatures of the constituent homopolymers. Although the  $\tan \delta$  curve of bPETBB14.3 did not contain a second prominent peak at a higher temperature, the weak shoulder at 103 °C (arrow in Fig. 1) was close to  $T_g$  of PETBB55. A small amount of transesterification, as indicated by NMR, could have accounted for slight shifts of about 2 °C from the transition temperatures of the homopolymers. Nevertheless, the relaxation behavior was consistent with a blocky structure for bPETBB14.3 and suggested that the PET and PETBB55 blocks were not miscible, but mainly phase-separated as PETBB55 domains in a PET matrix.

Heating thermograms of the quenched films showed an inflection at the glass transition, a cold-crystallization exotherm, and a melting endotherm (Fig. 2). The transition temperatures and transition enthalpies are compiled in Table 2.  $T_g$ 's from differential scanning calorimetry (DSC) were generally 4–5 °C lower than those from DMTA. Subsequent references to  $T_g$ , for example, in relation to the cold-draw temperature, refer to the DSC values. Equation 3 describes the copolymer  $T_g$ 's from DSC, with  $T_{g2}$  of PEBB taken to be 115 °C.

The thermal behavior of PET and PETBB55 was in agreement with previous reports. Both polymers crystallized readily from the glassy state; PETBB55 crystallized either from the glass or the isotropic melt more rapidly than PET to a comparable level of crystallinity, as measured by the melting enthalpy. The melting peak for PET was relatively sharp, whereas the melting peak of PETBB55 was broad and diffuse in agreement with the granular morphology previously observed for cold-crystallized PETBB55.<sup>20</sup> The correspondence in the enthalpies of crystallization and melting confirmed the amorphous nature of the quenched films (Table 2).

Quenched rPETBB14.3 film crystallized very slowly. The thermogram in Figure 2 shows a small cold-crystallization exotherm immediately preceding a small melting endotherm, which is 20 °C below the melting temperature of PET. The reluctance of rPETBB14.3 to crystallize was also apparent from the small crystallization exotherm in the cooling curve. However, a higher level of crystallinity, approaching that of PET, was achieved in rPETBB14.3 by isothermal crystallization at 155 °C for 4 h. These

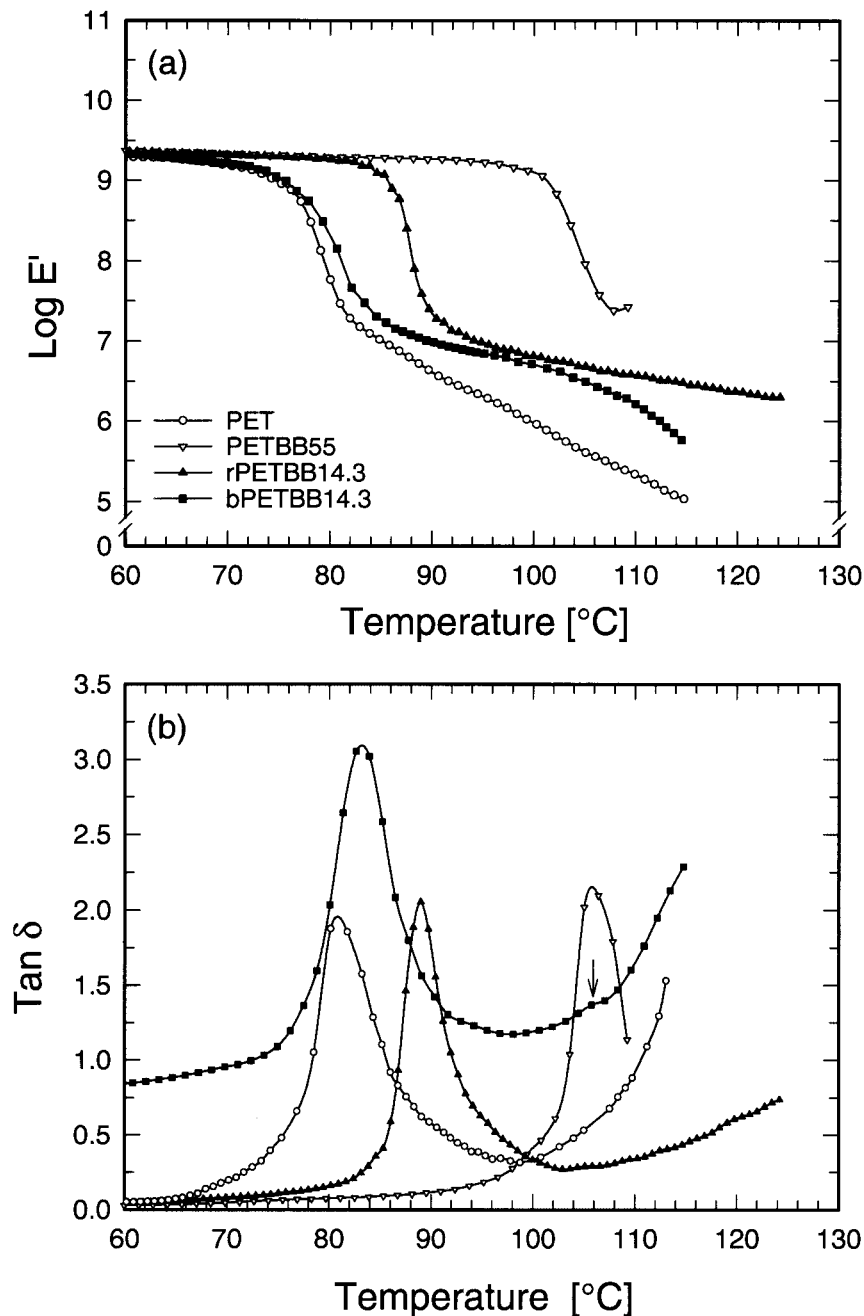


**Figure 1.** Dynamic mechanical behavior of quenched polyester films: (a)  $\log E'$ ; and (b)  $\tan \delta$ . The curve for bPETBB14.3 is shifted vertically.

observations were consistent with previous findings that copolymerization with less than 40 mol % bibenzoate retards the crystallization of PET, whereas copolymerization with more than 40 mol % accelerates the crystallization process.<sup>13</sup>

The crystallization of bPETBB14.3 was considerably different from that of rPETBB14.3, despite

the equivalence in the bibenzoate concentration. Thermograms of bPETBB14.3 closely resembled those of PET. The similarities extended to all aspects, including  $T_g$ , the temperature and enthalpy of cold crystallization and melting in the heating curve of the quenched glass, and the temperature and enthalpy of crystallization upon the cooling of the isotropic melt.

**Table 2.** Thermal Properties of Quenched Films

Material	DSC								
	DMTA	Heating						Cooling	
	$T_g$ (°C)	$T_g$ (°C)	$\Delta C_p$ (J g <sup>-1</sup> °C <sup>-1</sup> )	$T_{cc}$ (°C)	$\Delta H_{cc}$ (J g <sup>-1</sup> )	$T_m$ (°C)	$\Delta H_m$ (J g <sup>-1</sup> )	$T_c$ (°C)	$\Delta H_c$ (J g <sup>-1</sup> )
PET	81	77	0.302	142	-34	244	35	172	-33
PETBB55	106	101	0.300	116	-26	246	27	208	-25
rPETBB14.3	89	84	0.324	181	-9.0	223	9.5	154	-3.5
bPETBB14.3	83,103	78	0.341	148	-32	240	36	170	-32

$T_g$  is the glass transition temperature,  $\Delta C_p$  is the heat capacity change at  $T_g$ ,  $T_{cc}$  is the cold crystallization temperature,  $\Delta H_{cc}$  is the enthalpy of cold crystallization,  $T_m$  is the melting temperature,  $\Delta H_m$  is the melting enthalpy,  $T_c$  is the crystallization temperature, and  $\Delta H_c$  is the crystallization enthalpy.

WAXD patterns of isothermally crystallized films are shown in Figure 3. The triclinic crystal structure of PET is well known. The main diffraction peaks for a typical annealed PET film appear at  $2\theta = 16.3^\circ$  (011),  $2\theta = 17.6^\circ$  (010),  $2\theta = 21.6^\circ$  ( $\bar{1}11$ ),  $2\theta = 22.8^\circ$  ( $1\bar{1}0$ ), and  $2\theta = 26.1^\circ$  (100).<sup>21</sup> All of these were present in the WAXD pattern of the crystallized PET film, although they were not well resolved. Broad diffraction patterns are associated with relatively low crystallization temperatures of PET.<sup>21</sup> The crystal structure of PETBB55 has yet to be reported. The homopolymer PEBB crystallizes in a triclinic unit cell, with the main reflections at  $2\theta = 15.7^\circ$  (100),  $2\theta = 16.9^\circ$  ( $\bar{1}01$ ),  $2\theta = 24.1^\circ$  (010), and  $2\theta = 26.2^\circ$  (110).<sup>22</sup> Although the diffraction pattern of the PEBB crystal differs considerably, the chain configuration in the PEBB crystal resembles that of PET in many respects. Diffraction peaks of PETBB55 in Figure 3 corresponded to the  $2\theta$  values expected for PEBB, except that the (110) reflection shifted slightly from  $26.2$  to  $25.9^\circ$ , as observed previously.<sup>20</sup> The diffraction patterns of rPETBB14.3 and bPETBB14.3 were the same as the PET diffraction pattern. Although sequence analysis indicated that bPETBB14.3 retained the blocky structure after isothermal crystallization (Table 1), reflections characteristic of the PETBB55 crystal structure were not in evidence.

The combined observations from DSC and WAXD suggest that the manner in which bibenzoate is incorporated into PET profoundly influences the crystallization of the resulting copolymer. The random incorporation of 14.3 mol % bibenzoate greatly retards the crystallization of PET. At this concentration, bibenzoate units ap-

pear to be rejected from the PET crystal. If they are present in the crystal, they serve as defects. This is consistent with the slower rate of crystallization, the reduced enthalpy upon crystallization, and the 20 °C lower melting temperature of rPETBB14.3 in comparison with PET. In contrast, the same amount of bibenzoate incorporated into PET as PETBB55 blocks readily crystallizes with PET in the PET crystal structure without markedly altering the rate of crystallization, the enthalpy of crystallization, or the melting temperature.

The random copolymer from which the PETBB55 blocks were derived readily crystallizes in the PEBB crystal structure, which is a general feature of poly(ethylene terephthalate-co-bibenzoate) and poly(ethylene naphthalate-co-bibenzoate) with large amounts of bibenzoate.<sup>13,23</sup> However, in bPETBB14.3, both DSC and WAXD indicated that PETBB55 blocks did not crystallize as PETBB55, although the glass-transition behavior suggested that the PETBB55 blocks phase-separated in the glassy state. Therefore, despite it being present at a concentration of 30 wt %, neither crystallization and melting peaks attributable to PETBB55 nor X-ray reflections attributable to PETBB55 were evident. Instead, the blocky copolymer crystallized readily with PET. It is possible that the PETBB55 domains in bPETBB14.3 were too small for crystals to nucleate and grow independently, but the domains were readily incorporated into the PET crystal when the PET blocks crystallized. Although the diffraction patterns of crystalline PET and PETBB55 differ markedly, similarities in the crystal chain configuration support speculation that PETBB55 blocks are accommodated in the

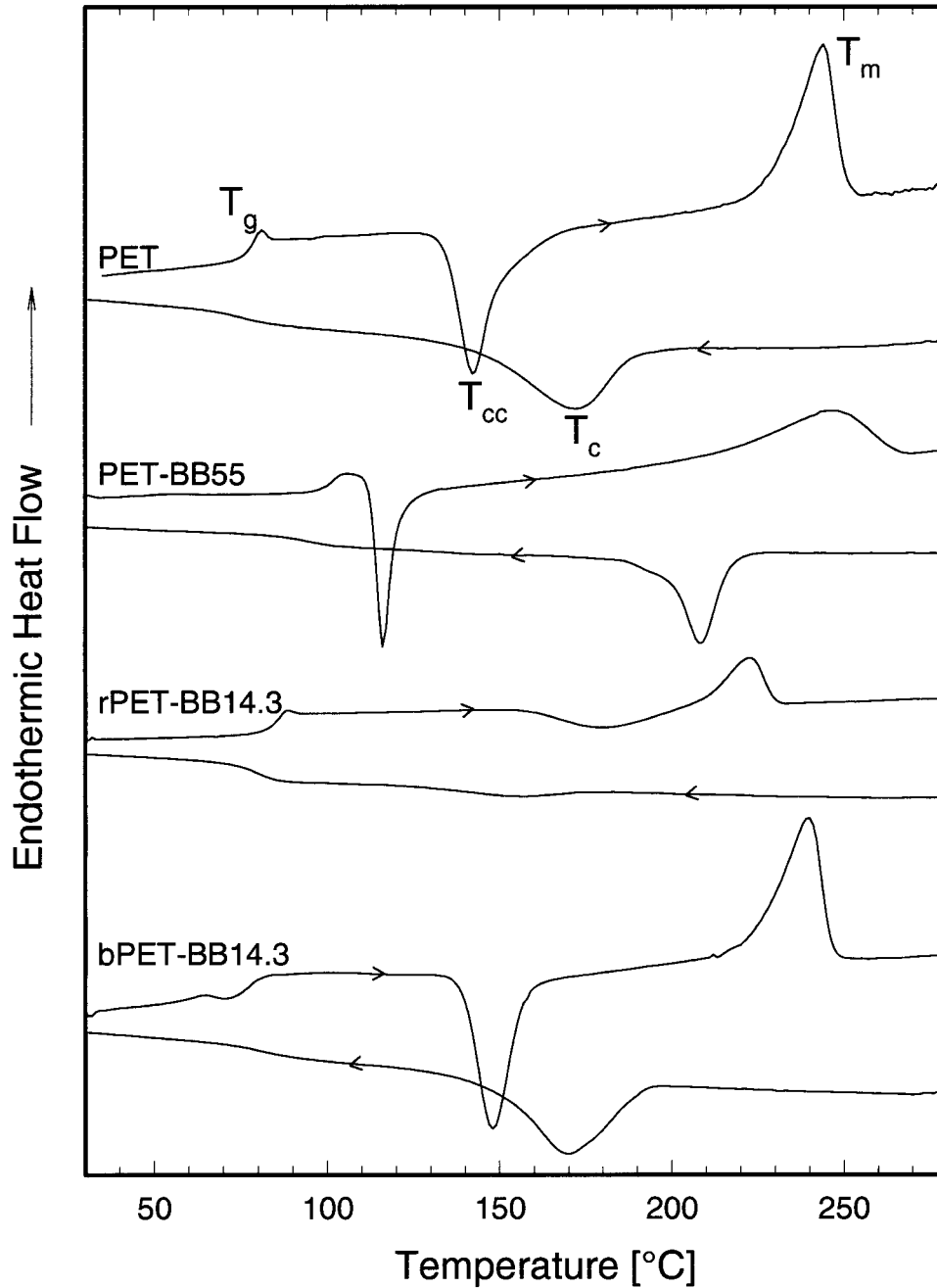


**Figure 2.** Heating and cooling thermograms of quenched polyester films. The heating and cooling rates were  $10\text{ }^{\circ}\text{C min}^{-1}$ .

PET unit cell. The small domain size also explains why the second  $T_g$  corresponding to the PETBB55 blocks is very weak.

#### Orientation by Cold Drawing

Quenched amorphous films were cold-drawn to a target draw ratio of 4 at various temperatures near  $T_g$  (Table 3). Orientation resulted in an

increase in density. The largest increase occurred with PETBB55, somewhat smaller increases occurred with bPETBB14.3 and PET, and the smallest increase in density occurred with rPETBB14.3 (Fig. 4). Cold drawing at higher temperatures tended to produce films with a smaller increase in density, which was attributed to relaxation during cold drawing.

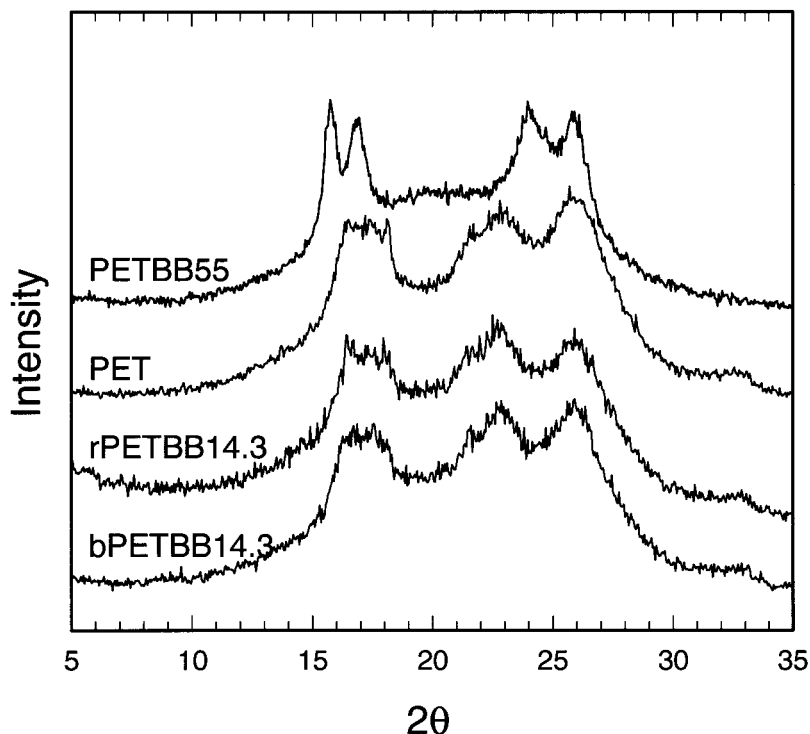


**Figure 3.** WAXD scans of polyester films isothermally crystallized at 155 °C for 4 h.

This was particularly evident with PET and rPETBB14.3. Indeed, rPETBB14.3 drawn at 120 °C (36 ° above  $T_g$ ) had a density of 1.3283 g cm<sup>-3</sup>, essentially the same density as the isotropic quenched film.

The blocky copolymer oriented much more readily than the random copolymer. Although the quenched films had virtually the same density (1.3304 and 1.3316 g cm<sup>-3</sup>), we could draw bPETBB14.3 at higher draw rates and achieve higher densities by cold-drawing over a larger temperature range in comparison with rPETBB14.3 (Table 3). Indeed, even at 120 °C (42 ° above  $T_g$ ), a density of 1.3522 g cm<sup>-3</sup> was achieved by the cold drawing of bPETBB14.3.

The densification of the glassy state through cold drawing near  $T_g$  results from the transformation of gauche glycol conformations into trans conformations.<sup>14</sup> Specific bands occur in three regions of the infrared spectrum of PET that are assigned to trans and gauche conformers: 1500–1400, 1400–1300, and 1000–800 cm<sup>-1</sup>.<sup>24–26</sup> The glycol regions of the PETBB55, bPETBB14.3, and rPETBB14.3 spectra closely resembled those of PET, and band assignments were made accordingly (Fig. 5).

The trans band at 1477 cm<sup>-1</sup> and the gauche band at 1457 cm<sup>-1</sup> were used for the quantitative determination of conformer populations (Fig. 6). Changes in the peak intensities revealed the expected increase in the trans conformers relative to the gauche conformers after orientation. Comparing spectra of rPETBB14.3 drawn at different temperatures, we found that the intensity of the trans band decreased slightly as the draw temperature was raised from 95 to 104 °C, and this was consistent with relaxation during drawing at the higher temperature. In contrast, the trans band of bPETBB14.3 did not change in intensity when the draw temperature was raised from 78 to 104 °C.

Spectra were normalized to the carbonyl band at about 1730 cm<sup>-1</sup>,<sup>27</sup> and the 1500–1400-cm<sup>-1</sup> region was deconvoluted into three Gaussian peaks to obtain the peak intensities.<sup>14</sup> The fractions of gauche and trans conformers were determined by the plotting of the normalized peak heights, as in Figure 7. Excellent linearity was obtained, and data for all the polymers followed the same relationship. Extrapolation gave intercepts that corresponded to the normalized band intensities for 100% trans and

**Table 3.** Oxygen Barrier Properties of Materials

Material	Draw Temperature (°C)	Draw Rate (mm min <sup>-1</sup> )	Draw Ratio	Density (g cm <sup>-3</sup> )	$P^a$	$D \times 10^{13}{}^b$	$S^c$	Trans Fraction	$\nu_f$ (cm <sup>3</sup> g <sup>-1</sup> )
PET									
$(T_g = 77\text{ °C})$	—	—	1.0	1.3370	$0.428 \pm 0.005$	$5.0 \pm 0.1$	$0.099 \pm 0.001$	0.09	0.027
	59	5	4.0	1.3539	$0.216 \pm 0.001$	$4.4 \pm 0.1$	$0.057 \pm 0.005$	0.27	0.018
	60 <sup>d</sup>	5	4.0	1.3535	0.203	4.0	0.058	0.26	0.018
	69	5	4.0	1.3537	$0.203 \pm 0.003$	$3.7 \pm 0.2$	$0.063 \pm 0.005$	0.26	0.018
	70 <sup>d</sup>	5	4.0	1.3537	0.203	3.7	0.063	0.27	0.018
	79	5	4.0	1.3540	$0.254 \pm 0.002$	$3.4 \pm 0.1$	$0.089 \pm 0.004$	0.28	—
	89	5	4.0	1.3485	$0.384 \pm 0.005$	$4.6 \pm 0.1$	$0.096 \pm 0.001$	0.20	—
PETBB55									
$(T_g = 101\text{ °C})$	— <sup>d</sup>	—	1.0	1.3073	$0.635 \pm 0.004$	$6.4 \pm 0.3$	$0.114 \pm 0.005$	0.07	0.030
	100 <sup>d</sup>	5	4.0	1.3354	0.147	3.1	0.055	0.39	0.014
	100 <sup>d</sup>	5	4.5	1.3371	$0.106 \pm 0.009$	$2.5 \pm 0.2$	$0.049 \pm 0.001$	0.40	0.013
rPETBB14.3									
$(T_g = 84\text{ °C})$	—	—	1.0	1.3304	$0.468 \pm 0.002$	$5.7 \pm 0.1$	$0.095 \pm 0.001$	0.09	0.029
	85	2	4.4	1.3389	0.136	2.0	0.079	0.25	0.024
	95	5	4.1	1.3420	0.192	2.8	0.080	0.28	0.022
	104	50	5.8	1.3360	0.309	3.7	0.096	0.19	0.025
	120	10	5.8	1.3283	0.504	5.3	0.109	0.10	0.030
bPETBB14.3									
$(T_g = 78\text{ °C})$	—	—	1.0	1.3316	$0.445 \pm 0.001$	$5.3 \pm 0.1$	$0.098 \pm 0.002$	0.08	0.028
	78	100	4.6	1.3525	0.130	2.5	0.060	0.35	0.016
	95	20	4.5	1.3547	0.143	2.9	0.057	0.36	0.015
	104	100	4.6	1.3578	0.137	3.0	0.053	0.38	0.013
	120	50	5.2	1.3522	0.227	3.7	0.072	0.31	—

<sup>a</sup> cc(STP) cm m<sup>-2</sup> day<sup>-1</sup> atm<sup>-1</sup>.<sup>b</sup> m<sup>2</sup> s<sup>-1</sup>.<sup>c</sup> cc(STP) cm<sup>-3</sup> atm<sup>-1</sup>.<sup>d</sup> From ref. <sup>14</sup>.

100% gauche conformers, respectively. The trans fraction  $f_t$  was defined as the following ratio:

$$f_t = \frac{A_t}{A_t^0} \quad (4)$$

where  $A_t$  is the normalized 1477-cm<sup>-1</sup> peak height and  $A_t^0$  is the normalized 1477-cm<sup>-1</sup> peak height for 100% trans conformers.  $f_t$  was about the same, 0.07–0.09, in all the quenched amorphous films (Table 3). However, for a target draw ratio of 4, it was possible to achieve significantly higher  $f_t$  values with bPETBB14.3 (almost 0.4) than with rPETBB14.3 (almost 0.3)

The relationship between  $f_t$  and density is plotted in Figure 8. The results for PET and PETBB55 were taken from a previous study in which the amount of orientation was varied by changes in the draw ratio.<sup>14</sup> Data for rPETBB14.3

and bPETBB14.3 defined a single linear relationship that was intermediate between the results for PET and PETBB55. Therefore, the higher density of cold-drawn bPETBB14.3 compared with that of rPETBB14.3 reflected a higher level of orientation, as measured by  $f_t$ . Extrapolation provided the density of 100% trans conformers as 1.412 g cm<sup>-3</sup> and the density of 100% gauche conformers as 1.320 g cm<sup>-3</sup>.

### Structural Model for Blocky and Statistical PETBB14.3 Copolymers

With the combined thermal, X-ray, and infrared results, it is possible to propose a structural model for the orientation of blocky bPETBB14.3 and statistical rPETBB14.3 that can explain the capacity of the blocky structure to achieve higher levels of orientation. In contrast to the homogeneous rPETBB14.3 glass [Fig. 9(a)], the

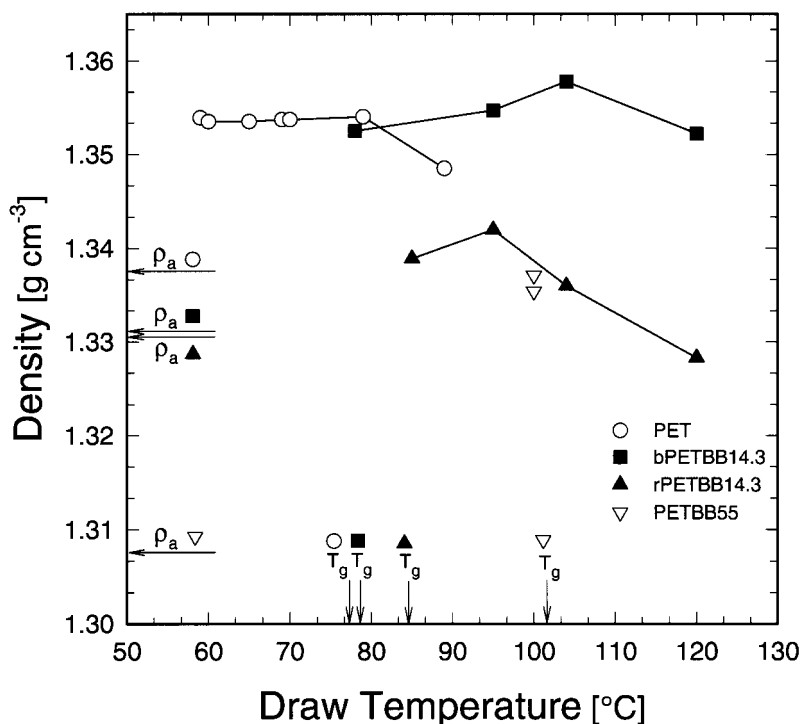


**Figure 4.** Density of drawn polyester films as a function of the draw temperature. The density of the quenched film is indicated on the y axis, and  $T_g$  is indicated on the x axis.

PETBB55 blocks of bPETBB14.3 appear to form separate domains in the amorphous glass [Fig. 9(b)]. This is indicated by the primary  $T_g$ , which is close to  $T_g$  of PET and significantly lower than  $T_g$  of rPETBB14.3 or the prediction from the copolymer equation (eq 3). However, the barely detectable  $T_g$  of the PETBB55 blocks suggests that the PETBB55 domains are very small. During cold crystallization, the PETBB55 domains appear to be readily incorporated into the PET crystal structure without significantly affecting the crystallization rate or the total crystallinity, whereas statistically distributed comonomer units effectively retard the crystallization rate of rPETBB14.3 and reduce the amount of crystallinity.

Homogeneous rPETBB14.3 readily relaxes if it is cold-drawn at a temperature that is above  $T_g$  at 84 °C [Fig. 9(c)]. This is evident from the lower density and lower trans glycol content of films drawn at temperatures above  $T_g$ . In comparison with rPETBB14.3, bPETBB14.3 can be oriented at higher draw rates and at higher draw temperatures. Indeed, bPETBB14.3 readily cold-draws at temperatures up to 104 °C, considerably above the primary  $T_g$  at 78 °C and approximately the  $T_g$  of the PETBB55 blocks, achieving high levels of

orientation, as indicated by the density and trans glycol content. It is speculated that the cold drawing of bPETBB14.3 produces highly oriented PETBB55 domains [Fig. 9(d)]. Covalent bonds, and possibly entanglements, connect the oriented PETBB55 blocks to the PET blocks that constitute the continuous phase. Constraints imposed by the connections prevent relaxation of the continuous phase. In this sense, the blocky copolymer approaches the concept of a self-reinforcing polymer.

### Oxygen Transport Properties

Typical experimental  $J(t)$  curves in Figure 10 describe  $J(t)$  through films of quenched and oriented rPETBB14.3. To facilitate comparisons among specimens that varied somewhat in thickness, we normalized the flux curves to a film thickness of 200  $\mu\text{m}$ . The careful conditioning and appropriate choice of the specimen thickness resulted in excellent resolution of the various features of the time dependence. The initial increase in  $J(t)$  reflected non-steady-state diffusion. This part of the curve was controlled mainly by  $D$ . As the permeant concentration in the specimen reached a constant distribution, the flux reached the steady-

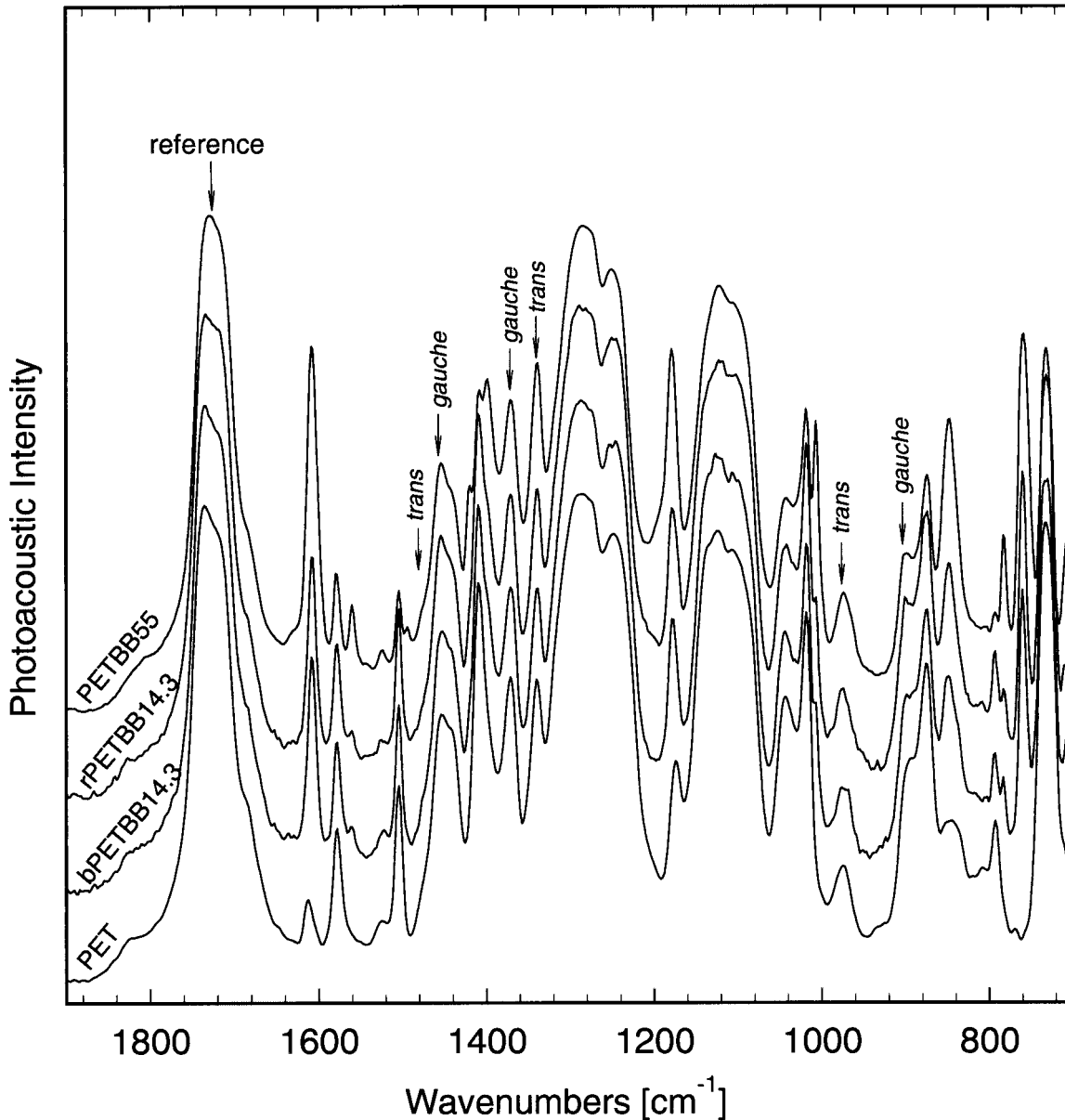


**Figure 5.** Photoacoustic Fourier transform infrared spectra of quenched polyester films.

state value  $J_0$ . This value, normalized to both the film thickness  $l$  and the permeant gas pressure  $p$ , defined  $P = J_0 l p^{-1}$ . Orientation affected both the non-steady-state and steady-state parts of the oxygen-flux curve. Typically, the non-steady-state region broadened (slower diffusion), and the flux decreased (lower permeability), as seen from a comparison of flux curves for the quenched film and the film drawn at 85 °C. Additional flux curves for rPETBB14.3 drawn at 95 and 104 °C showed a progressive increase in permeability as

relaxation at higher draw temperatures reduced the amount of orientation.

To obtain  $D$  and to accurately determine  $P$ , we fit the data to the solution of Fick's second law with appropriate boundary conditions:<sup>16</sup>

$$J(t) = \frac{Pp}{l} \left[ 1 + 2 \sum_{n=1}^{\infty} (-1)^n \exp\left(-\frac{D\pi^2 n^2 t}{l^2}\right) \right] \quad (5)$$

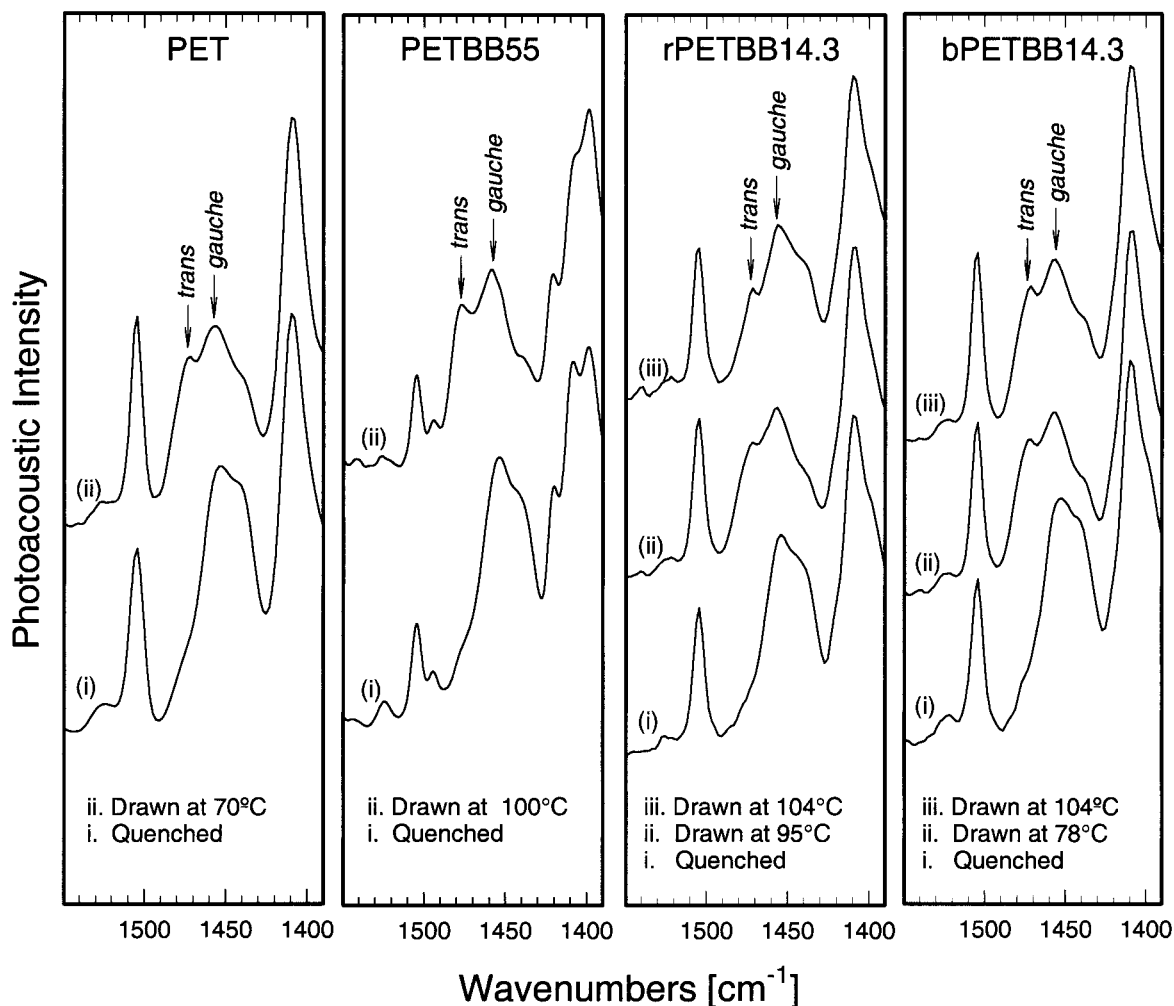


**Figure 6.** Effect of orientation on the 1500–1400-cm<sup>-1</sup> region of the infrared spectrum.

The fitting curves are included with the experimental points in Figure 10. The fit was equally good for all the experiments in the study. The error in determining the two fitting parameters,  $Pl^{-1}$  and  $Dl^{-2}$ , was estimated to be less than 2%. Therefore, the main source of error in calculating  $P$  and  $D$  from the experimental flux curves lay in the measurement of film thickness  $l$ . For this reason, special attention was paid to determining the average thickness. The bulk density method used for determining the average film thickness has been described previously.<sup>16</sup> Solubility  $S$  was calculated from the relationship  $S = PD^{-1}$ .

Oxygen permeability  $P$  of the cold-drawn polymers is plotted in Figure 11 as a function of the draw temperature. For a comparison of the effect of the draw temperature, the target draw ratio

was kept constant at 4, although this value was sometimes exceeded, especially in drawing at higher temperatures. One effect of a higher draw ratio would have been to increase the amount of orientation and correspondingly decrease the permeability. Alternatively, a higher draw temperature would have facilitated chain relaxation. In all cases, the lowest permeability was achieved through cold drawing at or below  $T_g$ . The reduced permeability of cold-drawn polymers was due to decreases in both  $D$  and  $S$  (Table 3).

After cold drawing, all the copolymers containing bibenzoate exhibited lower permeability than PET. This reversed the trend exhibited by quenched films, for which permeability was lowest for PET and increased with the amount of bibenzoate (Table 3). It followed that bibenzoate enhanced the effectiveness of cold drawing.

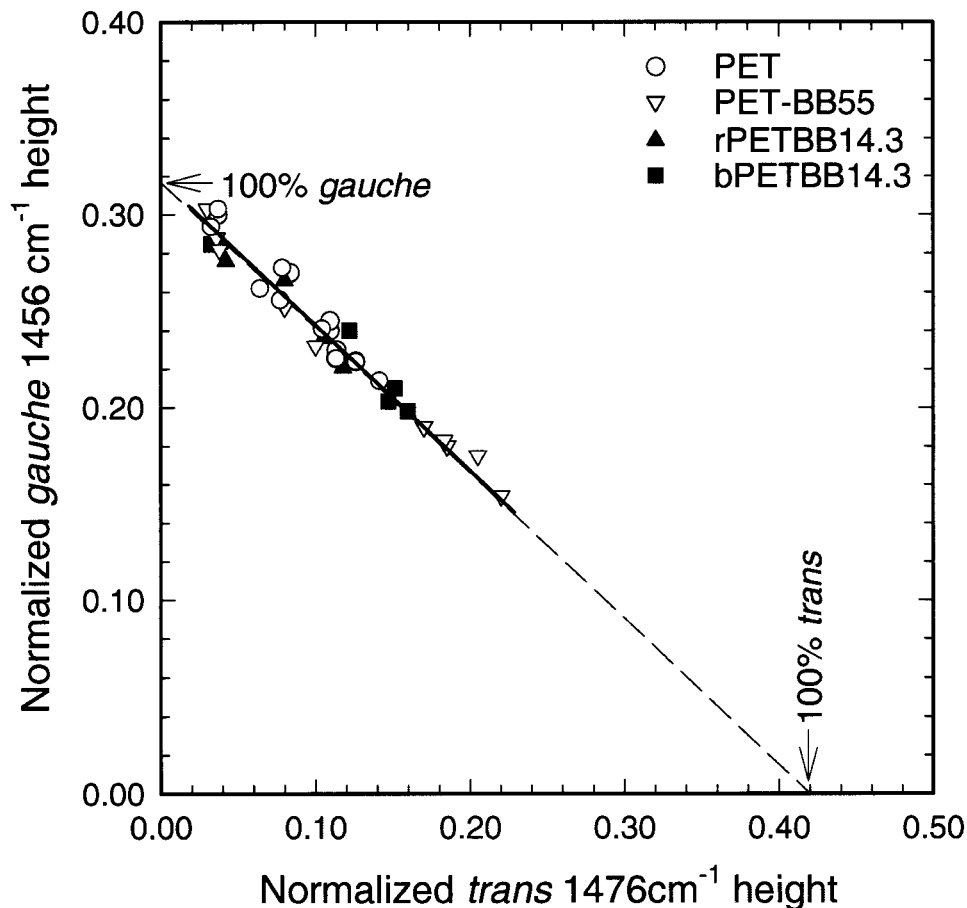


**Figure 7.** Normalized peak heights of the gauche and trans infrared bands. Additional data for PET and PETBB55 from ref. <sup>14</sup> are included.

Therefore, the barrier improvement with a target draw ratio of 4 was  $6\times$  in PETBB55,  $3.4\times$  in rPETBB14.3 and bPETBB14.3, and  $2.1\times$  in PET.

Permeability tended to increase gradually as the draw temperature was raised above  $T_g$ . Therefore, the permeability of PET increased from  $0.203 \text{ cc(STP) cm m}^{-2} \text{ day}^{-1} \text{ atm}^{-1}$  after drawing below  $T_g$  to  $0.384 \text{ cc(STP) cm m}^{-2} \text{ day}^{-1} \text{ atm}^{-1}$  after drawing at  $89^\circ\text{C}$  ( $12^\circ\text{C}$  above  $T_g$ ), which approached the permeability of isotropic amorphous PET of  $0.428 \text{ cc(STP) cm m}^{-2} \text{ day}^{-1} \text{ atm}^{-1}$ . Similarly, the permeability of rPETBB14.3 increased as the draw temperature was raised above  $T_g$ . In this case, the highest draw temperatures used resulted in permeability equal to or even slightly higher than the permeability of the isotropic amorphous polymer of  $0.468 \text{ cc(STP) cm m}^{-2} \text{ day}^{-1} \text{ atm}^{-1}$ ; that is, the temperature was high enough to enable complete relaxation during the cold drawing.

The exception to the trend was bPETBB14.3. Drawing at  $104^\circ\text{C}$  ( $26^\circ$  above  $T_g$ ) produced es-

entially the same low permeability [ $0.137 \text{ cc(STP) cm m}^{-2} \text{ day}^{-1} \text{ atm}^{-1}$ ] as cold drawing at  $78^\circ\text{C}$  [ $0.130 \text{ cc(STP) cm m}^{-2} \text{ day}^{-1} \text{ atm}^{-1}$ ]. Only at a draw temperature of  $120^\circ\text{C}$ , which was above the  $T_g$  of PETBB55, did the permeability increase to  $0.227 \text{ cc(STP) cm m}^{-2} \text{ day}^{-1} \text{ atm}^{-1}$ . This was evidence that the PETBB55 blocks stabilized orientation and enhanced resistance to chain relaxation.

#### Oxygen Solubility

A recent study demonstrates that a one-phase model is sufficient to describe the oxygen solubility of cold-drawn polyesters.<sup>14</sup> Cold drawing is viewed as increasing the density of the glassy polymer by transforming gauche conformers into trans conformers. A linear relationship between oxygen solubility  $S$  at 1 atm and specific volume  $\nu$  was demonstrated for cold-drawn PET, PEN, and PETBB55. More recently, this relationship was

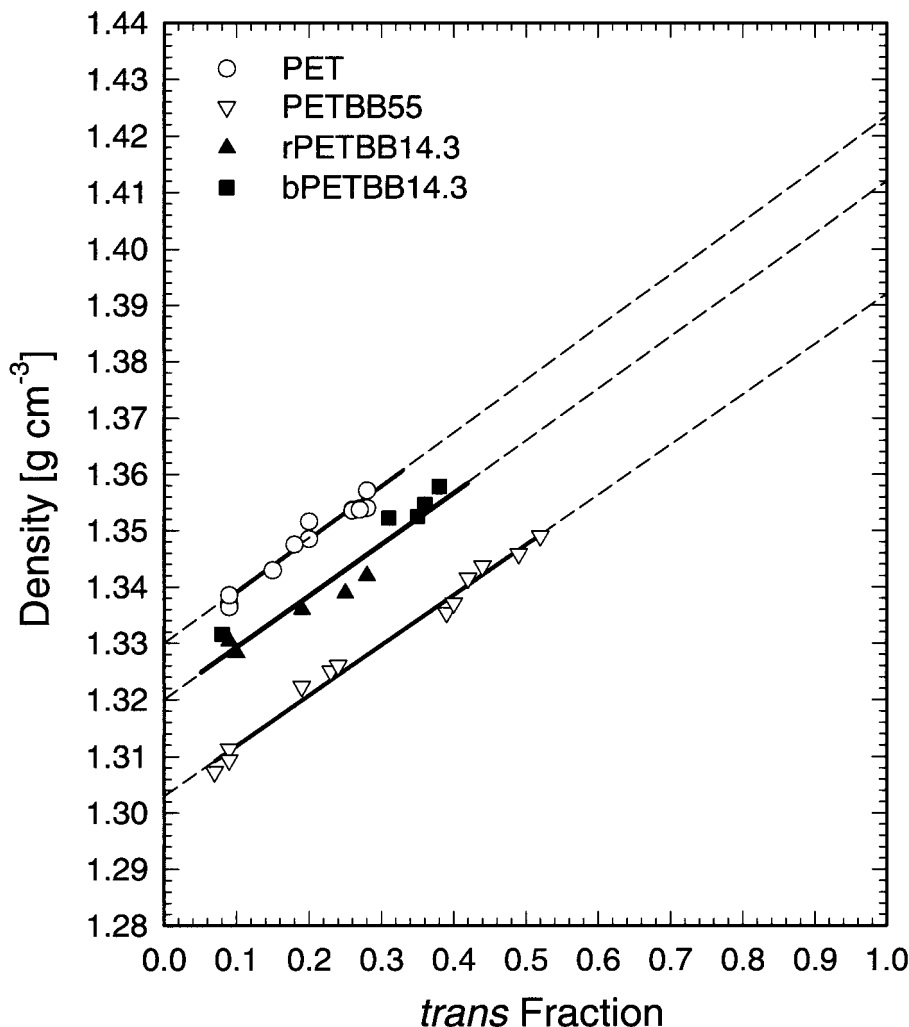


**Figure 8.** Relationship between the density and trans fraction. Additional data for PET and PETBB55 from ref. <sup>14</sup> are included.

demonstrated for copolymers of PET containing hydroquinone ether linkages.<sup>28</sup> The relationship also extends to the amorphous phase of crystallized polyesters.<sup>29,30</sup> The general correlation between  $S$  and  $\nu$  is expressed as follows:

$$S = \beta(\nu - \nu_0) \quad (6)$$

where  $\nu_0$  is the specific volume at zero solubility. According to free-volume concepts that view the sorption of small gas molecules as the process of filling holes of static free volume, the quantity  $\nu_f = \nu - \nu_0$  identifies the excess hole free volume available to oxygen.<sup>14</sup> The orientation of the glass decreases the excess hole free volume, whereas crystallization often has the effect of increasing the excess hole free volume of the amorphous phase. The extrapolated quantity  $\nu_0$  is not neces-

sarily the same for all polyesters and reflects a characteristic of the particular chemical structure. However, the slope  $\beta$  is about  $3.6 \text{ cc(STP) g cm}^{-6} \text{ atm}^{-1}$  for all the aromatic polyesters studied. The slope reflects the density of sorbed oxygen, and constant  $\beta$  indicates fundamental similarity in the characteristics of the accessible free volume in the glassy state.

The  $S$ - $\nu$  correlations in Figure 12 include results obtained previously for PET and PETBB55.<sup>14</sup> Data for drawn rPETBB14.3 and bPETBB14.3 fit a single linear relationship that fell between the results for PET and PETBB55. The linear fits had a common slope  $\beta$  of  $3.6 \text{ cc(STP) g cm}^{-6} \text{ atm}^{-1}$ . Extrapolation gave a  $\nu_0$  value of  $0.723 \text{ cm}^3 \text{ g}^{-1}$  ( $\rho = 1.383 \text{ g cm}^{-3}$ ) for rPETBB14.3 and bPETBB14.3. Results for PET drawn above  $T_g$  (79 and 89 °C) and results for bPETBB14.3 drawn at 120 °C are excluded be-

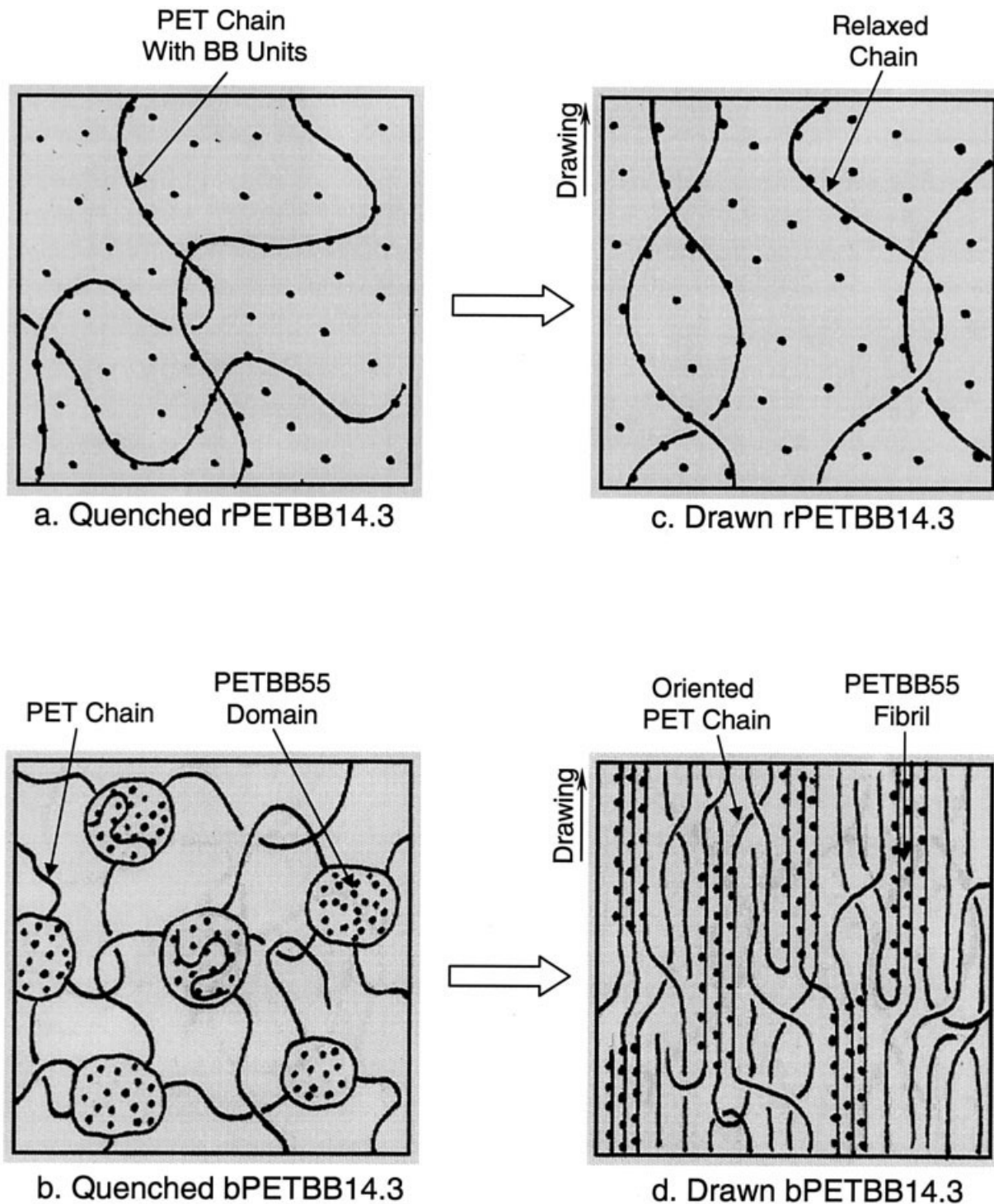


**Figure 9.** Proposed structural models for statistical and blocky copolymers: (a) rPETBB14.3 glass, (b) bPETBB14.3 glass, (c) rPETBB14.3 cold-drawn above  $T_g$ , and (d) bPETBB14.3 cold-drawn above the primary  $T_g$ . Bibenzoate units are indicated by dots.

cause of the possibility of strain-induced crystallization. These films exhibited higher solubility than cold-drawn films with approximately the same den-

sity, indicating the possibility of a crystalline phase and a dedensified amorphous phase.<sup>16</sup> Strain-induced crystallization was not a consideration for

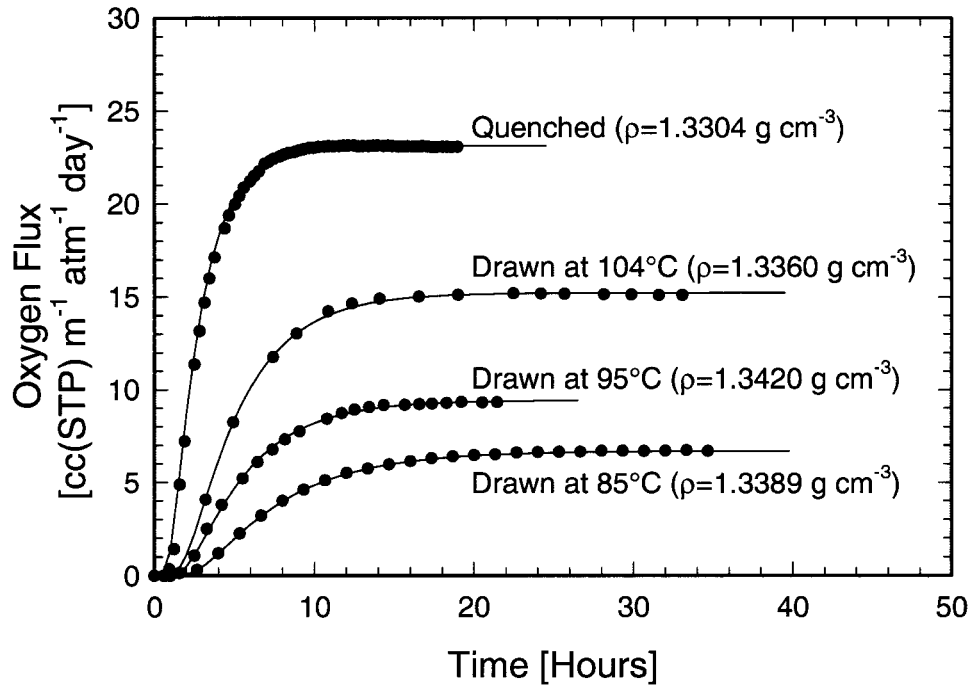


**Figure 10.** Experimental  $J(t)$  data fit to eq 5 for quenched rPETBB14.3 drawn at various temperatures.

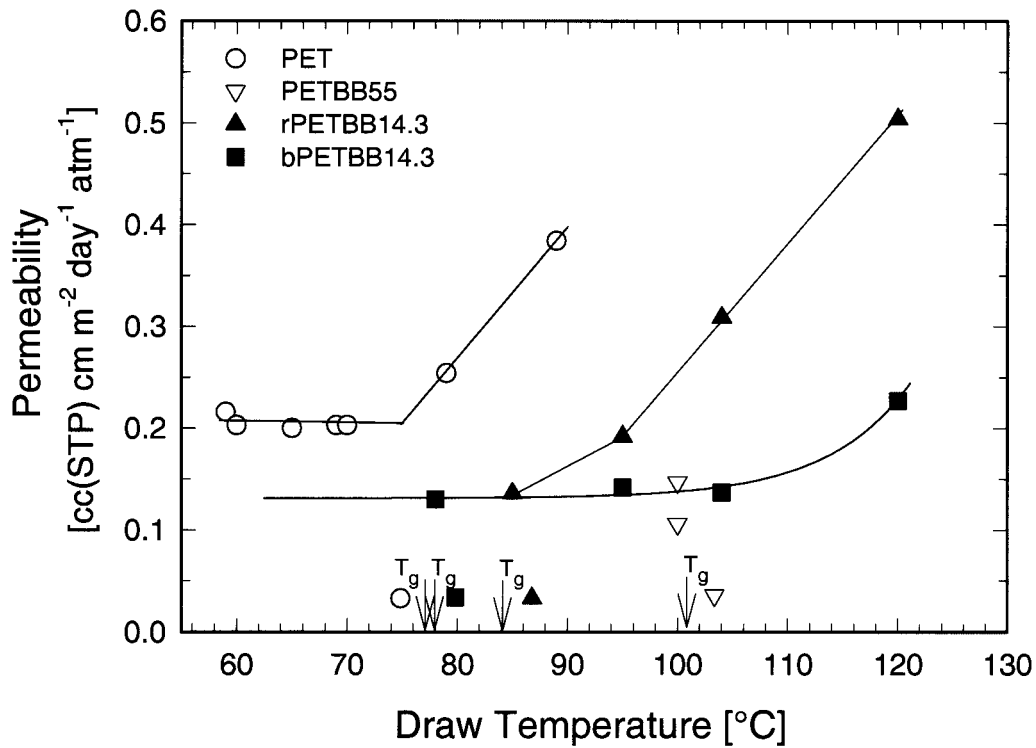


**Figure 11.** Effect of the draw temperature on the permeability for a target draw ratio of 4.  $T_g$  is indicated on the x axis.

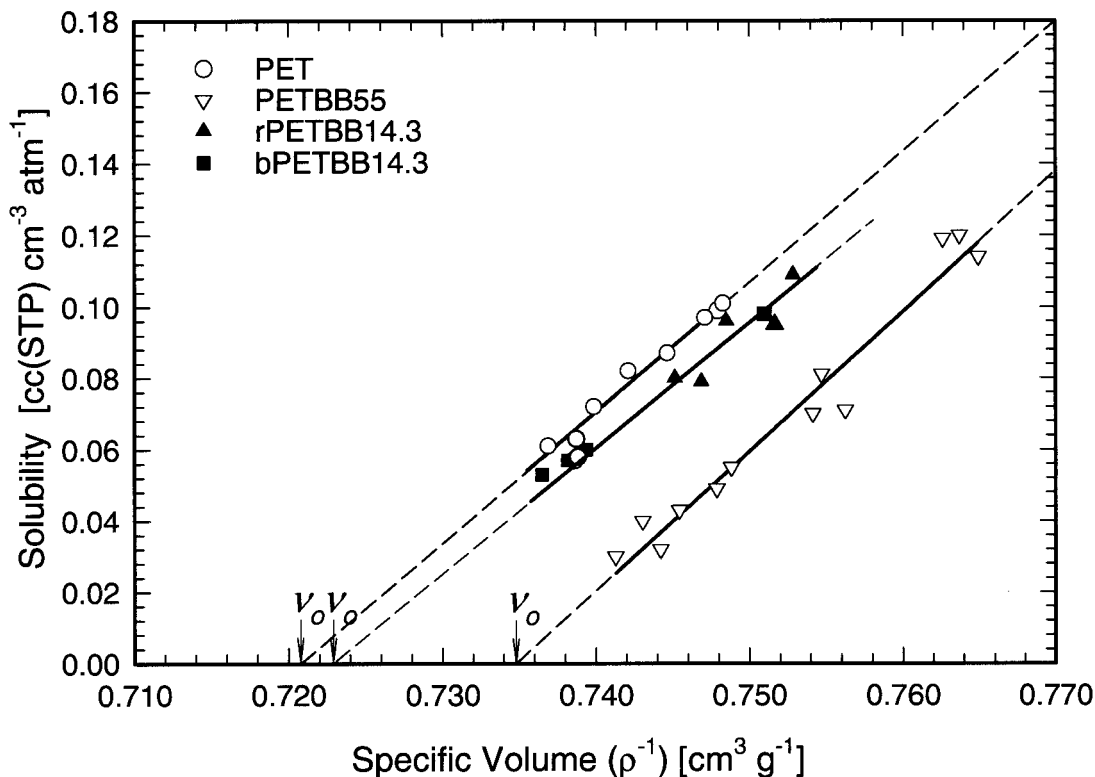


**Figure 12.** Relationship between the oxygen solubility and specific volume ( $\nu = \rho^{-1}$ ). Additional data for PET and PETBB55 from ref. <sup>14</sup> are included.

rPETBB14.3 because of its slow crystallization kinetics.

## CONCLUSIONS

The study demonstrates that the transesterification of two aromatic polyesters in melt blends is slow enough that the blend maintains a substantially blocky character during the normal processes of molding, cold drawing, and cold crystallization. In this way, frustrated LCP blocks of PETBB55 can be incorporated into PET. The separation of PETBB55 blocks as very small domains in the glassy state is thought to be responsible for major differences in the cold-crystallization and cold-drawing behaviors in comparison with the copolyester with a statistical comonomer distribution. It is speculated that the cold drawing of the blocky copolymer produces highly oriented PETBB55 domains. Constraints imposed by connections between PET and PETBB55 blocks prevent the relaxation of the continuous PET phase, even at temperatures well above the  $T_g$  of PET. The unusual cold-draw characteristics of the

blocky copolymer create an extended processing window, in terms of the draw rate and draw temperature, in which good barrier characteristics can be achieved.

Orientation significantly reduces oxygen permeability because of decreases in both solubility and diffusivity. Oxygen solubility at 1 atm of pressure correlates with the density and trans glycol fraction and, therefore, lends itself to a straightforward interpretation as filling holes of excess hole free volume. The process of orientation reduces the amount of excess hole free volume. Better orientation of the blocky copolymer compared with that of the random copolymer directly translates into lower oxygen solubility. Orientation also decreases oxygen diffusivity, but a one-to-one correlation with orientation, as measured by the density or trans glycol fraction, is not observed; indeed, the orientation of blocky and random copolymers produces about the same decrease in diffusivity. It is apparent that the kinetic contribution to permeability depends on factors other than excess hole free volume, such as local chain dynamics.

This research was generously supported by the National Science Foundation (DMR 9975774 and DMR 9986467) and KoSa. Support from Modern Controls, Inc., for the development of a facility for gas-transport studies at Case Western Reserve University is gratefully acknowledged.

## REFERENCES AND NOTES

- Polyakova, A.; Liu, R. Y. F.; Schiraldi, D. A.; Hiltner, A.; Baer, E. *J Polym Sci Part B: Polym Phys* 2001, 39, 1889–1899.
- Nagai, K.; Higuchi, A.; Nakagawa, T. *J Polym Sci Part B: Polym Phys* 1995, 33, 289–298.
- Morisato, A.; Freeman, B. D.; Pinnau, I.; Casillas, C. G. *J Polym Sci Part B: Polym Phys* 1996, 34, 2209–2222.
- Jarus, D.; Hiltner, A.; Baer, E. *Polymer* 2002, 43, 2401–2408.
- Brown, C. S.; Alder, P. T. In *Polymer Blends and Alloys*; Folkes, M. J.; Hope, P. S., Eds.; Blackie: Glasgow, 1993; Chapter 8, pp 193–227.
- Baird, D. G.; McLeod, M. A. In *Polymer Blends*; Paul, D. R.; Bucknall, C. B., Eds.; Wiley: New York, 2000; Vol. 2, Chapter 32, pp 429–453.
- Chiou, J. S.; Paul, D. R. *J Polym Sci Part B: Polym Phys* 1987, 25, 1699–1707.
- Weinkauff, D. H.; Kim, H. D.; Paul, D. R. *Macromolecules* 1992, 25, 788–796.
- Weinkauff, D. H.; Paul, D. R. *J Polym Sci Part B: Polym Phys* 1991, 29, 329–340.
- Miranda, N. R.; Willits, J. T.; Freeman, B. D.; Hopfenberg, H. B. *J Membr Sci* 1994, 94, 67–83.
- Li, X.; Brisse, F. *Macromolecules* 1994, 27, 2276–2282.
- Schiraldi, D. A.; Lee, J. J.; Gould, S. A. C.; Occelli, M. L. *J Ind Eng Chem* 2001, 7, 67–71.
- Ma, H.; Hibbs, M.; Collard, D. M.; Kumar, S.; Schiraldi, D. A. *Macromolecules* 2002, 35, 5123–5130.
- Liu, R. Y. F.; Schiraldi, D. A.; Hiltner, A.; Baer, E. *J Polym Sci Part B: Polym Phys* 2002, 40, 862–877.
- Schiraldi, D. A.; Occelli, M. L.; Gould, S. A. C. *J Appl Polym Sci* 2001, 82, 2616–2623.
- Sekelik, D. J.; Stepanov, S. V.; Nazarenko, S.; Schiraldi, D.; Hiltner, A.; Baer, E. *J Polym Sci Part B: Polym Phys* 1999, 37, 847–857.
- Qureshi, N.; Stepanov, E. V.; Schiraldi, D.; Hiltner, A.; Baer, E. *J Polym Sci Part B: Polym Phys* 2000, 38, 1679–1686.
- Martinez de Ilarduya, A.; Kint, D. P. R.; Munoz-Guerra, S. *Macromolecules* 2000, 33, 4596–4598.
- Herbert, I. R. In *NMR Spectroscopy of Polymers*; Ibbett, R. N., Ed.; Blackie: London, 1993; Chapter 2, pp 50–79.
- Hu, Y. S.; Rogunova, M.; Schiraldi, D. A.; Hiltner, A.; Baer, E. *J Appl Polym Sci* 2002, 86, 98–115.
- Bove, L.; D'Aniello, C.; Gorrasi, G.; Guadagno, L.; Vittoria, V. *Polym Adv Technol* 1996, 7, 858–862.
- Li, X.; Brisse, F. *Macromolecules* 2000, 33, 7529–7537.
- Wendling, J.; Gusev, A. A.; Suter, U. W.; Braam, A.; Leemans, L.; Meier, R. J.; Aerts, J.; Van der Heuvel, J.; Hottenhuis, M. *Macromolecules* 1999, 32, 7866–7878.
- Miyake, A. *J Polym Sci* 1959, 38, 479–495.
- Miyake, A. *J Polym Sci* 1959, 38, 497–512.
- Lin, S.-B.; Koenig, J. L. *J Polym Sci Polym Phys Ed* 1982, 20, 2277–2295.
- Cole, K. C.; Daly, H. B.; Sanschagrín, B.; Nguyen, K. T.; Aji, A. *Polymer* 1999, 40, 3505–3513.
- Andrade, G. S.; Collard, D. M.; Schiraldi, D. A.; Hu, Y. S.; Baer, E.; Hiltner, A. *J Appl Polym Sci*, in press.
- Polyakova, A.; Stepanov, E. V.; Sekelik, D.; Schiraldi, D. A.; Hiltner, A.; Baer, E. *J Polym Sci Part B: Polym Phys* 2001, 39, 1911–1919.
- Hu, Y. S.; Liu, R. Y. F.; Rogunova, M.; Schiraldi, D. A.; Nazarenko, S.; Hiltner, A.; Baer, E. *J Polym Sci Part B: Polym Phys* 2002, 40, 2489–2503.